Biosensors and Bioelectronics 58 (2014) 200–204

Contents lists available at ScienceDirect

Biosensors and Bioelectronics

journal homepage: www.elsevier.com/locate/bios

Short communication

Graphene oxide functionalized with silver@silica–polyethylene glycol hybrid nanoparticles for direct electrochemical detection of quercetin

Murugan Veerapandian [a,b], Yeong-Tai Seo [c], Kyusik Yun [a,*], Min-Ho Lee [d,**]

[a] Department of Bionanotechnology, Gachon University, Gyeonggi-Do 461-701, Republic of Korea
[b] Department of Chemistry, University of Montreal, CP 6128, Succursale Centre-ville, Montreal, QC H3C 3J7, Canada
[c] School of Electrical Engineering and Computer Science, Seoul National University, Seoul 151-600, Republic of Korea
[d] Korea Electronics Technology Institute, Medical IT Technology, Gyeonggi-Do 463-816, Republic of Korea

ARTICLE INFO

Article history:
Received 19 November 2013
Received in revised form
21 February 2014
Accepted 25 February 2014
Available online 5 March 2014

Keywords:
Graphene oxide
Chemical functionalization
Hybrid nanoparticles
Quercetin biosensor

ABSTRACT

A direct electrochemical detection of quercetin based on functionalized graphene oxide modified on gold-printed circuit board chip was demonstrated in this study. Functionalized graphene oxide materials are prepared by the covalent reaction of graphene oxide with silver@silica–polyethylene glycol nanoparticles (~12.35 nm). Functionalized graphene oxide electrode shows a well-defined voltammetric response in phosphate buffered saline and catalyzes the oxidation of quercetin to quinone without the need of an enzyme. Significantly, the functionalized graphene oxide modified electrode exhibited a higher sensitivity than pristine gold-printed circuit board and graphene oxide electrodes, a wide concentration range of 7.5 to 1040 nM and detection limit of 3.57 nM. Developed biosensor platform is selective toward quercetin in the presence of an interferent molecule.

1. Introduction

Quercetin is one of the abundant flavonoid molecules with a wide range of biological roles such as anti-oxidant (Zhou et al., 2001), anti-inflammatory, anti-allergic (Guardia et al., 2001; Rogerio et al., 2010), anti-cancer (Murakami et al., 2008) and anti-bacterial activity (Bravo and Anacona, 2001). Due to its polyhydroxy functional groups in the aromatic rings, quercetin (3,3′,4′,5,7-pentahydroxyflavone) is demonstrated to form a complex reaction with metal ions, influencing the transportation, reactivity, bioavailability and toxicity of metal ions (Dolatabadi, 2011). Transition metal complexes with quercetin are studied to have improved sequence-selective DNA binding and photochemical properties (Tan et al., 2009; Dolatabadi, 2011). Therefore, determination of quercetin with high sensitivity is of vital importance from therapeutics point-of-view. Recently, quercetin has been determined by spectrophotometry (Nikolovska-Coleska et al., 1996), high performance liquid chromatography (Wang et al., 2005), capillary electrophoresis (Prasongsidh and Skurray, 1998) and spectrofluorimetry methods (Liu et al., 2012). Later, electrochemical quercetin biosensors especially supported by nanomaterials were studied to have predominant advantages than conventional methods such as relatively rapid analysis time, simplicity in operation and low cost for fabrication of devices. For instance, multi-walled carbon nanotube (MWCNT) electrode (He et al., 2005), carbon nanotubes and nafion (Xu and Kim, 2006), monosuccinyl beta-cyclodextrin doped MWCNT (Jin et al., 2009) and Ag nanoparticles in ionic liquid and laccase immobilized on β-cyclodextrin modified with epichlorohydrin were developed for the determination of quercetin (Franzoi et al., 2010). Recently, successful determination of quercetin was demonstrated by using p-aminothiophenol functionalized graphene oxide/gold nanoparticles (Yola et al., 2013) and molecularly imprinted polymer with graphene oxide (Sun et al., 2013).

Modification of conventional electrodes with different nanostructures such as zero dimensional nanoparticles, one-dimensional nanotubes and two-dimensional graphene-materials has attracted a great deal of interest due to their heterogeneous composition and high surface-to-volume ratio with interesting electrochemical properties (Amal Raj et al., 2011; Lavanya et al., 2012; Palanisamy et al., 2013). Stability of hybrid nanomaterials modified at the electrode surface and binding affinity of analyte biomolecules on the electrode-material interface is highly depends on the physicochemical composition of hybrid nanomaterials. Recently, our group has constructed a new class of, three-dimensional nanostructure, functionalized graphene oxide (FGO) containing metalloid polymer hybrid (MPH) nanoparticles, which possess significant electrochemical properties (Veerapandian et al., 2012a). It has been explained that the FGO utilized for biosensing platform i.e., MPHs chemically conjugated (via the amidation process) on graphene oxide (GO), which is distinct from conventional composite film that are physically mixed or sequentially dropped on the electrode surface.

* Corresponding author. Tel.: +82 31 789 7549; fax: +82 31 789 7559.
** Corresponding author.
E-mail addresses: ykyusik@gachon.ac.kr (K. Yun), mhlee@keti.re.kr (M.-H. Lee).

http://dx.doi.org/10.1016/j.bios.2014.02.062
0956-5663

The strong affinity between chemically bonded hybrid particles and GO is expected to induce enhanced electron transfer kinetics and long term stability at the electrode interface. Furthermore, the MPHs are composed of three different chemical compositions, such as metal (silver, Ag), non-metal (silica, SiO_2) and polymer (polyethylene glycol, PEG), together as single nanocomposite particles.

In this communication, we demonstrate the FGO modified gold-printed circuit board (Au-PCB) electrode as a new class of biosensor platform for quercetin determination with a wide range of detection and high sensitivity. From this present study, our results showed that FGO modified electrode is significantly responsive toward the electrocatalysis of quercetin and required no additional supporting matrix on the electrode surface-interface. This approach is attractive not only for new system but also for convenient in fabrication and operation of quercetin biosensing platform.

2. Experimental

2.1. Chemicals

Silver nitrate ($AgNO_3$), tetraethoxysilane (TEOS) ($Si(OC_2H_5)_4$), sodium borohydride ($NaBH_4$), ammonium hydroxide (NH_4OH), poly(ethylene glycol) (PEG) (average M_n=10,000), 3-aminopropyltriethoxysilane (3-APTES), expandable graphite powder and quercetin were purchased from Sigma-Aldrich. Sulfuric acid (H_2SO_4), potassium permanganate ($KMnO_4$), hydrogen peroxide (H_2O_2), hydrochloric acid (HCl) and anhydrous ethanol (C_2H_5OH) were obtained from Daejung Chemicals and Metal Ltd., Republic of Korea. The 2 μM quercetin stock solution was prepared in ethanol and utilized for preparation of further solutions. Phosphaste-buffered saline (PBS, Sigma-Aldrich) was used as the common electrolyte solution for all electrochemical measurements, prepared by dissolving 1 tablet of PBS (Sigma-Aldrich) in 200 mL of deionized water, which gives a final concentration of 0.0027 M potassium chloride and 0.137 M sodium chloride, pH 7.4 at 25 °C. All the chemical reagents were of analytical grade and used as received without further purification.

2.2. Synthesis of GO nanosheets

Aqueous colloidal dispersions of GO nanosheets were synthesized by vigorous oxidation of graphite powder following the modified Hummers method (Hirata et al., 2004).

2.3. Synthesis of MPHs

MPHs composed of Ag@SiO_2–PEG with an average particle size distribution of ~12.35 nm were synthesized following an ultrasonochemistry (Veerapandian and Yun, 2010a). Briefly, an aqueous solution of a metal precursor $AgNO_3$ (30 mM) was added to a reaction vessel containing PEG (stabilizing agent) solution and 30 mM of $NaBH_4$ (reducing agent). The reagent mixture was kept under probe ultrasonicator for a period of 15 min, with an optimized conditions such as amplitude (35%), probe temperature (65 °C) and pulse on–off cycle (5–10 s), in order to form the Ag core. Following this, the desired 30 mM TEOS and NH_4OH were simultaneously added. The reaction vessel was again underwent ultrasonication for a period of 30 min to ensure complete reduction and formation of the hybrid structure. The resulting colloidal dispersions containing hybrid nanoparticles were separated by centrifugation. As-separated nanoparticles were washed twice with ethanol and deionized water and were utilized for further experimentation.

2.4. Synthesis of FGO nanosheets

MPHs were first silanized and then covalently reacted with oxygenated functional groups of GO nanosheets, following a procedure detailed elsewhere (Veerapandian et al., 2012a). Briefly, an aqueous dispersion of MPHs (5 mg mL^{-1}) and 3-APTES (30 μL mL^{-1} in C_2H_5OH) was added to a vial containing 3 mL of anhydrous C_2H_5OH. This was kept under magnetic stirring at 800 rpm in room temperature for a period of 10 h. Subsequent to this, an aqueous solution of GO (2.5 mg mL^{-1}) was added and kept under magnetic stirring at 800 rpm for another 10 h to facilitate a covalent reaction between silanized MPHs and GO. After this reaction period, the GO functionalized with MPHs were separated by centrifugation, washed thrice with ethanol and used for construction of the Au-PCB modification.

2.5. Construction of Au-PCB-GO or Au-PCB-FGO electrode for quercetin detection

Prior to surface modification, Au-PCB electrode substrate was sequentially washed with acetone, ethanol and deionized water. Following this, the Au-PCB electrode was exposed to oxygen plasma treatment for ~2 min. Then, typically, 5 μL of aqueous GO or FGO suspension (2 mg mL^{-1}) was drop casted and allowed to evaporate at ambient temperature for 1 h. As-fabricated Au-PCB electrodes were then utilized for further electrochemical measurements.

A custom-designed Au-PCB substrate with an area of ~2 mm in diameter (circle shaped) was used as the working electrode and the two crescent-shaped Au substrates with a length of 4.3 mm and a breadth of 0.8 mm were used as counter and reference electrodes, respectively. Digital photograph for an Au-PCB electrode was shown in Supplementary information (Fig. S3).

2.6. Instrumentation

UV–visible absorbance spectra were measured from a Varian Cary 50 UV–vis spectrometer. Raman spectra were recorded with a LabRam HR800 micro-Raman spectroscope (Horiba Jobin-Yvon, France) using 100× objective lens at room temperature, with a 532 nm Nd:YAG laser beam and 1800 lines per mm grating. High resolution transmission electron microscope (HR-TEM) images of GO and FGO were obtained from Cs-corrector equiped HR-TEM (FEI Titan 80-300) operated at 300 kV. Cyclic voltammograms (CVs) and linear sweep voltammograms (LSVs) were measured using VersaSTAT 3 (Princeton Applied Research) in a three electrode configuration.

3. Results and discussion

3.1. Characterization of functionalized graphene oxide nanostructures

Fundamental surface topography and optical properties of GO and FGO nanosheets were characterized by HR-TEM micrographs and UV–vis absorption spectrum. As observed from Fig. 1(a) FGO nanosheet shows significant surface modification with well-distributed hybrid nanoparticles. Especially a higher number of nanoparticles functionalized on the edge plane, indicating that the existence of carboxyl groups (at the edge plane) has predominantly involved in the covalent reaction (amidation process) with silanized-MPHs. On the other hand, the pristine GO nanosheet (Fig. 1(a), inset) reveals the transparent sheet morphology with wrinkles and corrugated texture. The HR-TEM image of MPHs and its respective size distribution histogram graph were shown in

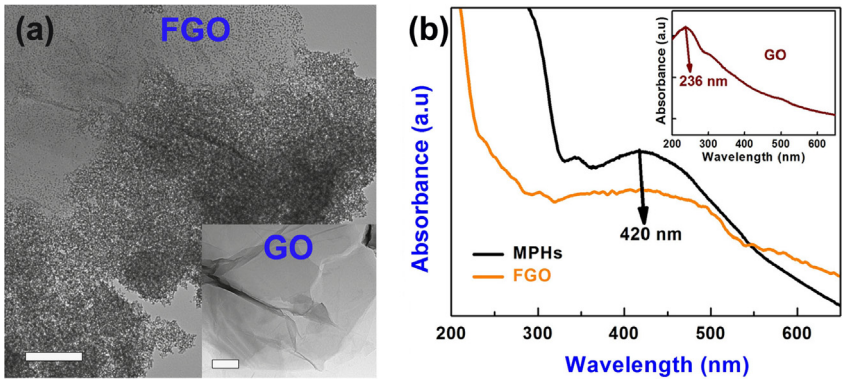

Fig. 1. (a) HR-TEM image of FGO (scale bar=500 nm) and GO (scale bar=200 nm) nanosheets. (b) UV–vis absorption spectrum of MPHs and FGO nanosheets (inset shows the spectrum of GO).

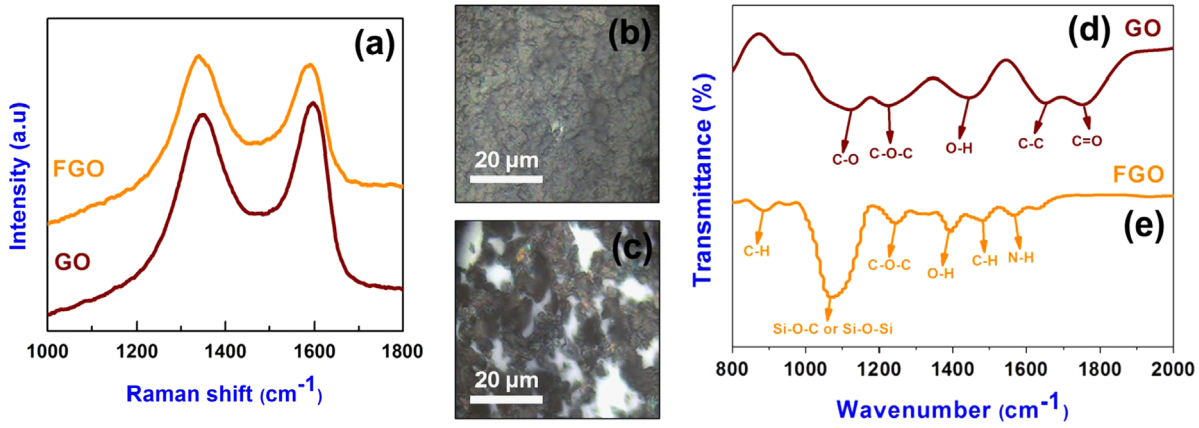

Fig. 2. (a) Raman spectrum of GO and FGO, and optical microscope image of (b) GO and (c) FGO nanosheets. FT-IR spectrum of (d) GO and (e) FGO nanosheets.

Figs. S1 and S2. The UV–vis spectrum of GO (Fig. 1b, inset) shows a wavelength of maximum absorbance at ~236 nm attributed to the π–π* of the C–C aromatic rings (Veerapandian et al., 2012a). After reacting with MPHs, the absorption spectrum of FGO showed a broad spectrum around ~420 nm (Fig. 1b) suggesting that MPHs were significantly modified on the surface of GO nanosheet. Due to the fact that surface of Ag core was modified with two different layers such as SiO_2 and PEG, the optical absorbtivity of MPHs localized on the surface of GO is certainly weakened. However observed absorbance supported the successful surface modification on GO nanosheet, this result is agreed well with the previous reports (Veerapandian et al., 2012a,2012b).

Raman spectroscopic measurement was performed to understand the fundamental carbon lattice information such as vibrations of sp^2-hybridized carbon atoms (G-band) and vibrations of carbon atoms with dangling bonds in plane terminations of disordered graphite (D-band) (Krishnamoorthy et al., 2012). As shown in Fig. 2(a) the Raman spectrum of FGO nanosheets was observed to have slight blue-shift in their D-band (1341 cm^{-1}) and G-band (1590 cm^{-1}) compared to pristine GO nanosheets (D-band: 1347 cm^{-1} and G-band: 1597 cm^{-1}). The ratio of D- to G-band intensity ($I_{(D)}/I_{(G)}$) for FGO nanosheet (1.02) was calculated to be slightly higher than that for GO nanosheet (0.95), ensuring that the surface functionalization of GO with silanized-MPHs was considerably altered the lattice structures of FGO nanosheets (Shen et al., 2011). Chemical structures of GO nanosheet such as carbonyl (C–O, 1050 cm^{-1}), epoxyl (C–O–C, 1250 cm^{-1}), carboxyl associated O–H bending vibrations (1413 cm^{-1}), C–C stretching (1623 cm^{-1}) and carboxylic acid stretching (1731 cm^{-1}) were identified (Fig. 2d). The FT-IR spectrum of FGO nanosheet shown in Fig. 2e exhibits significant alterations in the stretching and bending vibrations than pristine GO nanostructures such as C–H rocking signals (892 cm^{-1}), asymmetric stretches of organic Si–O–Si or Si–O–C (1080 cm^{-1}), epoxyl group frequency (1243 cm^{-1}), O–H bending vibrations (1392 cm^{-1}), asymmetric/symmetric C–H bending signal (1479 cm^{-1}) and furthermore appearance of a new group frequency (1569 cm^{-1}), attributed to the secondary amine N–H bending (Veerapandian and Yun, 2010b). These structural informations supported the successful covalent functionalization of GO with silanized-MPHs.

3.2. Electrochemical detection of quercetin

Our previous investigations (Veerapandian et al., 2012a) demonstrated that the GO functionalized with MPHs produced a well-defined redox wave in PBS buffer with a better electrocatalytic response than Au-PCB electrode for glucose monitoring. Here, the direct, i.e., support-less or reagent free, detection of quercetin was performed using the Au-PCB electrode modified with FGO nanosheets. Distinctly the Au-PCB electrode has been integrated into two crescent shaped substrates, which were used as reference and counter electrodes, respectively (see Supplementary Fig. S3). This electrode design was pretty compact and convenient for commerical device developments. Fig. 3(a) shows the comparative LSV of three different electrodes such as pristine Au-PCB, Au-PCB-GO and Au-PCB-FGO nanosheets under PBS buffer (pH 7.4) at a scan rate of 50 mV/s, without quercetin. It has been observed that there was no significant voltammetric peak appeared for pristine Au-PCB. LSV of Au-PCB electrode modified with GO nanosheet only exhibits an exponential variation of intensity vs. potential. On the other hand, FGO electrode showed the well-defined voltammetric peak centered at $E_{pa}=+0.32$ V attributed to the MPHs

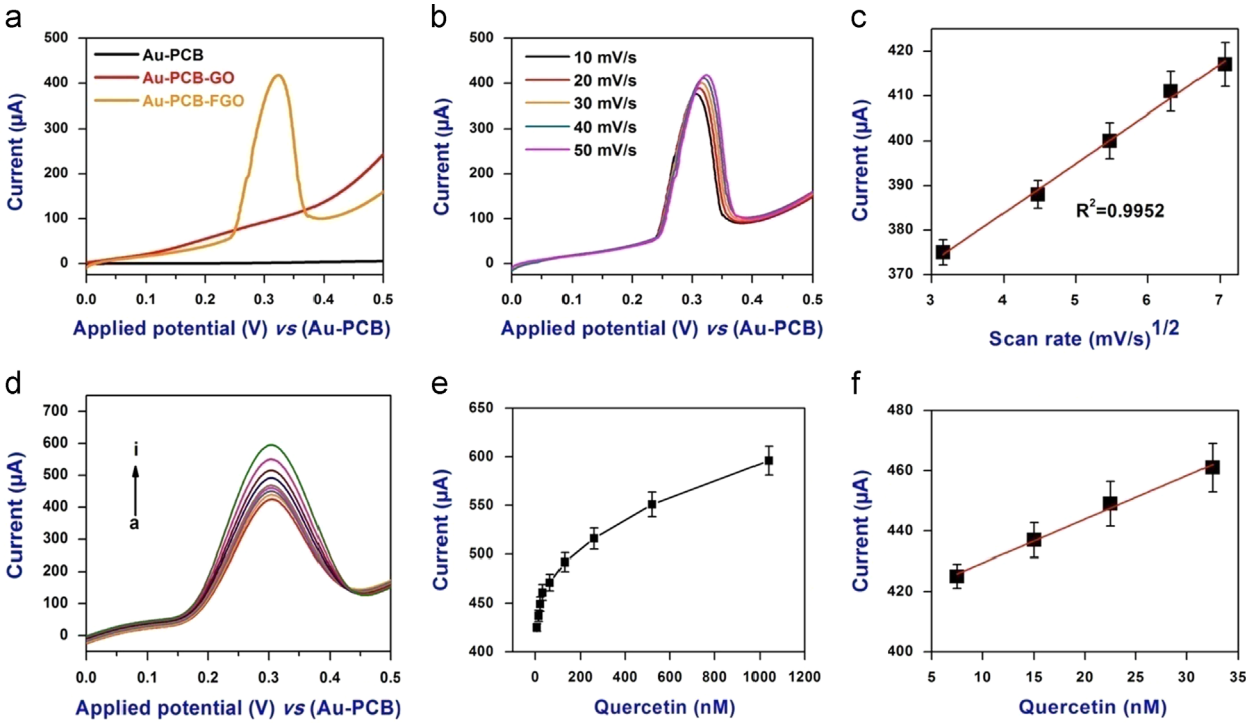

Fig. 3. (a) LSV of Au-PCB, Au-PCB-GO and Au-PCB-FGO electrode measured under PBS (pH 7.4) at a scan rate of 50 mV/s. (b) LSVs of Au-PCB-FGO electrode at various scan rates from 10 to 50 mV/s and (c) its respective peak currents plot vs square root of scan rate. (d) LSV of Au-PCB-FGO electrode against various concentrations of quercetin dissolved in PBS (pH 7.4), at a scan rate of 50 mV/s (a=7.5, b=15, c=22.5, d=32.5, e=65, f=130, g=260, h=520 and i=1040 nM). (e) Linear response of steady state current with quercetin for the Au-PCB-FGO electrode and (f) the linearity at a low concentration. Illustrated error bars represent the standard deviation of three measurements analyzed with a single electrode at each concentration.

(Ag@SiO_2–PEG) functionalized on the surface of GO nanosheets. Since there was no redox chemical species from the solution directly involved, the voltammetric oxidation reaction observed on LSV ascribed to MPHs functionalized on GO nanosheet. It is worth to mention that GO nanosheet provided an active interface matrix or support to MPHs and retained their stability throughout the reaction, due to chemically bonded with silanized-MPHs. Presence of PEG coating layer at the electrode interface was reported to have a significant role in affinity between biomolecules and electrode (Sung and Bae, 2003).

Mechanism of redox wave generation from Ag nanoparticles (NPs) or Ag doped amino SiO_2 nanostructures modified on metal electrodes have been proposed to be $Ag \rightarrow Ag_2O$ and $Ag_2O \rightarrow Ag$ at +0.37 V and −0.03 V, (Wang et al., 2004; Chang et al., 2005; Guo et al., 2008) respectively. It has been demonstrated that when AgNPs were embedded by aminosilica film it promotes the electron transfer rate by its smallest difference of oxidation and reduction potential (Choi and Luo, 2011). Likewise, in the present case hybrid nanostructure composed of Ag core, SiO_2 shell and PEG layer together into one single nanoplatform bonded with GO provided an enhanced electron transfer reaction at the electrode interface. CVs (Figs. S4–S6 in Supplementary results) of three different electrodes in the presence and absence of quercetin molecules provide an insight into the redox difference between Au-PCB-FGO and pristine Au-PCB/Au-PCB-GO electrodes. The scan rate dependence of the LSV response from FGO electrode was examined (Fig. 3b) and found that the anodic peak is proportional to the square root of the scan rate ($\upsilon^{1/2}$) with a correlation co-efficient of 0.9952 (Fig. 3c), suggesting that the electrode reaction is controlled by the diffusion.

Structure of quercetin exhibits five OH groups, which can undergo oxidation reaction and its pH-dependence (Brett and Ghica, 2003). It has been observed that these OH groups can generate four anodic peaks at +0.15, +0.30, +0.60 and +0.80 V. Among which the anodic peaks at +0.15 and +0.30 V are observed to be stable for various pH conditions and exhibit increased peak currents especially at neutral pH (Brett and Ghica, 2003). Interestingly in this study the FGO electrode is also studied to have an anodic peak potential at nearly +0.32 V. It is therefore possible to detect the analyte quercetin through its inherent elctrochemical oxidation reaction at the FGO electrode interface, without requiring additional reagent. From Fig. 3d, it can be seen that in the presence of quercetin in PBS solution (pH 7.4), the anodic peak current produced from the FGO electrode has slight shift in their potential region at E_{pa}=+0.30 V (from E_{pa}=+0.32 V, in Fig. 3a: Au-PCB-FGO trace). This ensures the active electron transfer between the electrode substrate and analyte (quercetin) molecules. In other words, FGO material modified on the electrode surface has significantly catalyzed the electrooxidation of quercetin into quinone. Furthermore, the voltammetric response of FGO electrode linearly responds to quercetin concentration. Under optimized conditions the linear range of response from present FGO electrode was observed to be 7.5 to 1040 nM (Fig. 3e). The limit of detection and current sensitivity were estimated to be 3.57 nM and 1.45 μA μM^{-1}, respectively (Fig. 3f). Selectivity of the FGO electrode was evaluated in the presence of mixture of quercetin and different concentrations of ascorbic acid (such as 0.26, 0.52 and 1.04 μM) (Fig. S7). Addition of various concentrations of ascorbic acid to electrolyte containing quercetin does not affect the inherent oxidation peak current of Au-PCB–FGO with quercetin, due to the fact that oxidation peak potential of ascorbic acid is located at different potential region than the prepared Au-PCB-FGO. Further, quercetin's oxidation potential is located within the FGO's anodic peak potential region, thus FGO is found to be a suitable electrochemical material for determination of oxidation of quercetin. Our present study, demonstrated that the electrodes modified with FGO nanosheets composed of chemically functionalized MPHs

on GO nanosheet resulted in a much lower detection limit of quercetin (see Supplementary Table S1). Unlike other physically adsorbed hybrid composite nanostructures the stability of current chemically-integrated FGO nanosheets are quite durable for long term analysis. Therefore, the FGO nanosheets modified electrode is very suitable for designing direct electrochemical biosensing of quercetin with high sensitivity.

4. Conclusion

We have described a simple surface modification of Au-PCB electrode with FGO nanosheets and demonstrated the direct electrochemical detection of quercetin. Owing to the uniform distribution and large surface-to-volume ratio of MPHs functionalized on the surface of GO resulted that FGO nanosheets modified on Au-PCB electrode shows much better performance to electrooxidation of quercetin, when compared with pristine Au-PCB/Au-PCB-GO electrodes. The strategy described herein enabled a lowest detection limit of 3.57 nM quercetin. Further, FGO modified electrodes does not require additional biomembrane and extensive sample pretreatment, therefore, will find potential applications in quantification of quercetin molecules.

Acknowledgment

This work was supported by GRRC program of Gyeonggi Province [2013-B02, fluorescence nanoparticle and liquid crystal sensor] and R&D Program funded by Ministry of Trade, Industry, and Energy [Grant no. 10045220].

Appendix A. Supporting information

Supplementary data associated with this article can be found in the online version at http://dx.doi.org/10.1016/j.bios.2014.02.062.

References

Amal Raj, M., Brillians Revin, S., Abraham John, S., 2011. Colloids Surf B. 87, 353–360.
Bravo, A., Anacona, J.R., 2001. Transit. Metal Chem. 26, 20–23.
Brett, A., Ghica, M.-E., 2003. Electroanalysis 15, 1745–1750.
Chang, G., Zhang, J., Oyama, M., Hirao, K., 2005. J. Phys. Chem. B 109, 1204–1209.
Choi, Y.J., Luo, T-J.M., 2011. Int. J. Electrochem. 404937, 1–6.
Dolatabadi, J.E.N., 2011. Int. J. Biol. Macromol. 48, 227–233.
Franzoi, A.C., Vieira, I.C., Scheeren, C.W., Dupont, J., 2010. Electroanalysis 22, 1376–1385.
Guardia, T., Rotelli, A.E., Juarez, A.O., Pelzer, L.E., 2001. Farmaco 56, 683–687.
Guo, L., Nie, J., Du, B, Peng, Z, Tesche, B, Kleinermanns, K., 2008. J. Colloid Interface Sci. 319, 175–181.
He, J.-B., Lin, X.-Q., Pan, J., 2005. Electroanalysis 17, 1681–1686.
Hirata, M, Gotou, T, Horiuchi, S, Horiuchi, S., Fujiwara, M., Ohba, M., 2004. Carbon 42, 2929–2937.
Jin, J.H., Kim, H., Jung, S., 2009. Biotechnol. Lett. 31, 1739–1744.
Krishnamoorthy, K., Veerapandian, M., Kim, G.S., Kim, S.J., 2012. Curr. Nanosci. 8, 934–938.
Lavanya, N., Radhakrishnan, S., Sekar, C., 2012. Biosens. Bioelectron. 36, 41–47.
Liu, J.M., Lin, L.P., Wang, X.X., Cai, W.L., Zhang, L.H., Lin, S.Q., 2012. Anal. Chim. Acta 723, 76–82.
Murakami, A., Ashida, H., Terao, J., 2008. Cancer Lett. 269, 315–325.
Nikolovska-Coleska, Z., Klisarova, L.J., Suturkova, L.J., Dorevski, K., 1996. Anal. Lett. 29, 97–115.
Palanisamy, K., Thandavarayan, M., Sahoo, N.G., Opallo, M., 2013. J. Mater. Chem. B 1, 4655–4666.
Prasongsidh, B.C., Skurray, G.R., 1998. Food Chem. 62, 355–358.
Rogerio, A.P., Dora, C.L., Andrade, E.L., Chaves, J.S., Silva, L.F.C., Lemos-Senna, E., Calixto, J.B., 2010. Pharmacol. Res. 61, 288–297.
Shen, J., Yan, B., Shi, M., Ma, H., Li, N., Ye, M., 2011. J. Colloid Interface. Sci. 356, 543–549.
Sun, S., Zhang, M., Li, Y., He, X., 2013. Sensors 13, 5493–5506.
Sung, W.J., Bae, Y.H., 2003. Biosens. Bioelectron. 18, 1231–1239.
Tan, J., Wang, B., Zhu, L., 2009. Bioorg. Med. Chem. 17, 614–620.
Veerapandian, M., Yun, K.S., 2010a. Langmuir 26, 14216–14222.
Veerapandian, M., Yun, K.S., 2010b. Synth. React. Inorg. Met-Org. Nano-Met. Chem. 40, 56–64.
Veerapandian, M., Lee, M.-H., Krishnamoorthy, K., Yun, K.S., 2012a. Carbon 50, 4228–4238.
Veerapandian, M., Seo, Y.-T., Shin, H., Yun, K.S., Lee, M.-H., 2012b. Int. J. Nanomed. 7, 6123–6136.
Wang, Y., Cao, J., Weng, J.H., Zeng, S., 2005. J. Pharm. Biomed. 39, 328–333.
Wang, G.F., Li, M.G., Gao, Y.C., Fang, B., 2004. Sensors 4, 147–155.
Xu, G.R., Kim, S., 2006. Electroanalysis 18, 1786–1792.
Yola, M.L., Atar, N., Ustundag˘, Z., Solak, A.O., 2013. J. Electroanal. Chem. 698, 9–16.
Zhou, J., Wang, L., Wang, J., Tang, N., 2001. Transit. Met. Chem. 26, 57–63.